PERGAMON

International Journal of Plasticity 17 (2001) 513–536

INTERNATIONAL JOURNAL OF Plasticity

www.elsevier.com/locate/ijplas

Intergranular and intragranular behavior of polycrystalline aggregates. Part 1: F.E. model

Fabrice Barbe [a], Luc Decker [b], Dominique Jeulin [b], Georges Cailletaud [a,*]

[a] *Centre des Matériaux/UMR 7633, Ecole des Mines de Paris/CNRS, BP87, F-91003 Evry, France*
[b] *Centre de Morphologie Mathématique, Ecole des Mines de Paris, 35 rue Saint Honoré, F-77305 Fontainebleau, France*

Received in final revised form 16 May 2000

Abstract

The constitutive equations currently used for metallic materials are written on a macroscopic scale, using macroscopic criteria and internal stresses to represent hardening. The granular nature of the material is then not represented. Since it may be critical in some cases, many attempts have already been made to account for it. So a series of modeling have been made in the framework of models having uniform stress or strain in each (crystallographic) phase. As a result, each crystallographic orientation has a different stress–strain state, but the actual microstructure is generally not introduced (Taylor model, self-consistent approach), so that the heterogenity obtained is not realistic. The aim of this work is to have a better evaluation of the heterogenity of stress and strain fields in realistic polycrystalline aggregates. For that purpose, an aggregate model is generated, and computed by finite element technique. The paper is presented in two parts, the first one being devoted to the description of the numerical tools, the second one showing the results at different scales. The present part includes the description of the 3D generator of microstructures, able to define any number of grains in a given 3D volume, with arbitrary shapes, and with a monitoring of the volume fraction of each phase. The result of this code will be taken as a starting point of the modeling, which is performed with a crystallographic model implemented in a parallel finite element code. Typical validation results are shown, with convergence data, on the size of the meshes and on the geometrical realisations of aggregates.

Keywords: A. Microstructures; B. Crystal plasticity; B. Inhomogeneous material; B. Polycrystalline material; C. Finite element

* Corresponding author. Tel.: +33-1-60-76-30-56; fax: +1-33-60-76-31-50.
E-mail address: gc@mat.ensmp.fr (G. Cailletaud).

0749-6419/01/$ - see front matter
PII: S0749-6419(00)00061-9

1. Introduction

Classical mechanical models are built after introducing the concept of representative volume element (RVE). The polycrystalline RVE is a material piece which must include a ''sufficient'' number of grains, in terms of crystallographic orientation, shape and size. The size of the RVE will depend of course on the typical lengths of the microstructure, and on the statistical distribution of the properties. In this case, a unique strain tensor and a unique stress tensor represent the material, forgetting on a macroscale the effect of the heterogenities. Authors usually refer to this type of stress as level 1 stress field. Level 2 corresponds to the mean value in a given phase of the material, which can be measured by X–ray diffraction with a spot including many grains, level 3 to the local value inside each grain, accounting for transgranular gradients.

Having access to the variation of the strain and stress fields on a microscale (level 3) can be useful for understanding the plasticity mechanisms and the crack initiation process. It has to be noted that the microstructural observations made by SEM or TEM concern this level. The aim of this paper then, is to generate a realistic 3D grain morphology and to apply constitutive equations describing crystal plasticity in each grain, by means of a finite element code, to characterise the heterogenity of these fields. This first approach concerns only spherical grain shapes, with only one chemical phase in each grain. The crystallographic orientation is the only character defining a ''phase'', and we will use isotropic textures, loaded in small deformations. Due to the neighborhood effect, two grains belonging to the same crystallographic class can have a different response. In the computations, it is assumed that the local behavior is uniform in each grain. On the other hand, a large number of degrees of freedom are introduced to account for the strong gradients in the grains. Having in hand these types of results, one can be interested in several types of analyses:

- global volume average produces stress–strain curve on the RVE (level 1);
- volume average on each phase (i.e. each set of grains belonging to the same crystallographic orientation class) produces local information which can be compared to Taylor or self–consistent approach (level 2). This analysis preserves the constitutive equations of each phase, but ''forgets'' the neighborhood effect;
- volume average on each individual grain gives some information at an intermediate scale, where the effect of the real morphology is present, but not the transgranular fields (no grain boundary effect);
- the local analysis of the stress and strain field is the only one which preserves both the local behavior and the local load balance, and which can give a realistic evaluation of the heterogenity inside the material.

The F.E. analysis of crystalline solids is now classical in the literature. The constitutive equations used can either describe single crystal or polycrystal behavior. The case of the single crystal can be considered to investigate the local behavior of bicrystalline specimens (Méric et al., 1994) or multicrystalline specimens with a low

number of grains (Havlicek et al., 1990; Teodosiu et al., 1991; Havlicek et al., 1992; Yao and Wagoner, 1993; Becker and Panchanadeeswaran, 1995; Harder, 1999). An intense activity can be expected in this field for the next decade, since it is now possible to get local strain fields (instead of discrete measurements) from the experimental observations. Another possible application of this type of computation is to deduce the global behavior of a polycrystal from elementary behavior of its grains. This type of application started more than 20 years ago (Engel, 1978; Gotoh, 1978). Since intensive computational resources are needed to achieve the computation, the field is still very active. Most of the time, the papers concern computations of polycrystals at large strains. Several types of meshes have been used by the authors. Many papers simply introduce a squared or a cubic mesh, each element corresponding to a different crystallographic orientation (Havlicek et al., 1992; Kalidindi et al., 1992; Takahashi et al., 1994; Beaudoin et al., 1995; Bertram et al., 1998; Bachu and Kalidindi, 1998; Dawson and Marin, 1998; Takahashi et al., 1998). This method is convenient to provide results concerning the global response of the aggregate. Still, it cannot provide any information on the local behavior, and has nothing to do with the real microstructure. A more precise modeling of the grain shape has also been proposed, with cylinders having a hexagonal section in quasi-3D computations (Harren and Asaro, 1989; Becker, 1991), or dodecahedra (Mika and Dawson, 1999). This approach has allowed the authors to investigate the local behavior at a transgranular level.

The viscoplastic approach proposed by Asaro (Asaro, 1983) is the most common model used for the single crystal with a simple interaction matrix, which is often reduced to a Taylor assumption (isotropic hardening) (Becker, 1991; Beaudoin et al., 1993; Mika and Dawson, 1998, 1999; Staroselski and Anand, 1998). More complex models, considering the dislocation-dislocation interaction, have also been used (Teodosiu et al., 1991; Harder, 1999). To account for anisotropic effects of the hardening in the slip systems, self-hardening and latent-hardening of the slip system resistances can be used (Bachu and Kalidindi, 1998). Kinematic hardening can be seen to simulate cyclic- and cross-loading tests (Takahashi et al., 1998). As well, twin has been introduced (Staroselski and Anand, 1998) to model the behavior of materials with low stacking fault energy like α-brass. In this case, latent hardening laws have been used for slip and twin resistance.

The original points of the present paper are first to consider 3D realistic morphologies, then to use a specific crystallographic model accounting for viscoplasticity, isotropic and kinematic hardening, and to focus on the small strain levels. At this stage of the deformation, the redistribution effect is already present, but not saturated, so that it is possible to compare the F.E. results with sophisticated models like self–consistent approach instead of considering a Taylor model. Besides, a detailed analysis of the intragranular level will be proposed.

In a recent paper (Quilici and Cailletaud, 1999), a brief presentation of the methodology was made, and initial results concerning the behavior in the core of the material were given. A comprehensive description of the methods has now been given, the second part of the paper (Barbe et al., 2001) being devoted to the study of the intragranular contours and the surface effect.

The first section of the present part describes the numerical tools used to generate a polycrystalline aggregate. Later the models for single crystal and polycrystal plasticity are presented. Section 3 provides a description of the numerical aspects of the model implementation, including both the parallel F.E. code and the small simulation code for the equivalent polycrystal model. In order to illustrate the influence of the numerical parameters of major importance in the definition of a polycrystal, several realisations, either with geometrical variations on the morphology of the microstructure or with different sets of textures, are presented in Section 4. Afterwards, Section 5 is devoted to the study of the convergence of the simulations with respect to the discretisation used, in terms of macroscopic responses compared to the responses of a homogenisation model.

2. Polycrystal generation

2.1. Models of random polycrystals

To account for the heterogenity of polycrystalline structures, a model of random medium, namely of random tesselation, has to be used. Every class of the tesselation will reproduce a metallic grain with a given crystallographic orientation and/or mechanical constitutive equations, according to the definition of phases in this paper.

The Voronoï polyhedra model (Gilbert, 1962) is a good candidate to generate random polycrystals, for geometrical considerations, since it provides planar boundaries separating grains, and because it reproduces some morphogenetic process, where germs grow with a constant and isotropic growth rate from random seeds. It was already used by Canova et al. (1992) in its standard version and with a limited number of crystals (100 in the mentioned reference). A more general model, reproducing germination and growth models is provided by the Johnson and Mehl model (1939), which can be simulated with slight changes of the present algorithm. To generate such microstructures, we propose an original method, with numerous extensions of the classical model (Decker and Jeulin, 2000). Its main advantages, as compared to standard procedures, is to be able to generate texture with a very large number of grains with a low computational cost, as explained below. Formally, Voronoï polyhedra are defined as zones of influence of a particular set of points, corresponding to their centers. Let $D \subset R^3$ and $E = \{A_i\}$ be a set of N random points $P(x, y, z)$ corresponding to the centers of grains in the continuous domain D. If $d(P_1, P_2)$ is the euclidean distance between two points P_1 and P_2, the zone of influence of a point A_i is defined in (1) by the set of points $P(x, y, z)$ with:

$$iz(A_i) = \left\{P(x, y, z) \in D | d(P, A_i) < d\left(P, A_j\right) \forall j \neq i\right\} \tag{1}$$

In more physical terms, a point P belongs to the zone of influence of germ A_i, if it is closer to A_i than to any other germ. By construction, this zone of influence

generates the Voronoï polyhedron centered in A_i. The set of zones of influence $\{iz(A_i)\}$ builds a random tesselation of the domain D into N classes, every A_i being the germ of one class.

Centers of polyhedra are usually obtained by simulating a Poisson point process, resulting in a uniform location inside the domain D (their coordinates are obtained as independent uniform random variables). Other distributions of germs can be simulated, as illustrated below. Polyhedra are immediately known from their boundaries (or faces), resulting from intersections of median planes of all segments connecting nearest neighbors (A_i, A_j). Building polyhedra with a common face is equivalent to looking for the solution of the dual problem of the Delaunay graph connecting the center of any polyhedron to the centers of its neighbors. In three dimensions, the determination of the solution of this problem by means of computational geometry is rather prohibitive when the number of germs N is larger than a few hundreds. Therefore, we have proposed a new approach.

2.2. Construction of Voronoï polyhedra on a grid of points

A specific procedure was developed to build Voronoï polyhedra inside a discrete domain, made of a 3D voxel map. The polyhedra are generated at a given resolution, defined by the size of the three-dimensional domain. We have to assign to each voxel the number (or label) of the grain to which it belongs. The generation of polyhedra is, therefore, obtained with a given spatial resolution, according to the size of the resulting image. For a given size, the precision of the definition of grain boundaries depends on their average volume, and, as a consequence, on the number of grains.

In a first step, a germination process gives the locations (on the grid) of the centers of grains. Then the Euclidean distance function of this set of points (Gratin, 1992, 1993) is calculated from an isotropic propagation starting from points. This process can be interpreted as a growth starting from every germ. The result can be displayed as a grey level image where the value in each point is proportional to the distance to the nearest source. This is illustrated in Fig. 1a for the case of a single source and in Fig. 1b for a set of point sources. The calculation of the distance function is implemented in a very efficient way, using the hierarchical queues algorithm (Meyer, 1990; Gratin and Meyer, 1992; Gratin, 1993; Ragnemalm, 1992), which enables us to

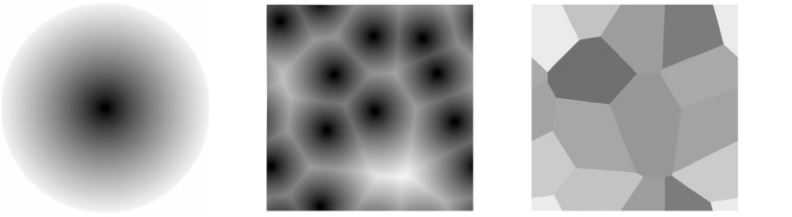

a) Distance function of a single point source

b) Distance function of a set of point sources

c) Final result after construction and labelling

Fig. 1. Construction of Voronoï polyhedra on a periodic grid (2D example).

produce simulations in a short time. The memory space needed for simulations is reasonable, although an intermediary 3D image with floating data is required (63 Mb are used for a domain with 180^3 voxels). The boundaries of polyhedra (as in Fig. 1c) can be obtained by two different ways. In the first method, the image of distances is considered as a topographical relief and the grain boundaries are obtained as the divide surfaces of the watersheds (a watershed being associated to each center). They are built by the "relief immersion" algorithm (Meyer and Beucher, 1990; Meyer, 1992). In the second method, the boundaries are obtained during the step of the calculation of the distance, if any voxel is assigned the label of its closest source.

This construction can be a first step in an analytical construction of polyhedra, using information on neighboring grains contained in the discrete 3D image. The calculation of intersection of planes is then obtained easily and it is possible to obtain coordinates of vertices of polyhedra, from which a finite element mesh may be generated. In the present paper, the mesh is made of a network of cubes as in (Canova et al., 1992).

Times to generate random tesselations are short, and can be neglected as compared to finite element calculations. The complexity of calculation is practically proportional to the number of voxels (and does not depend on the number of polyhedra). For indication, using a PC computer with the Linux OS (133 MHz, 64 Mb memory), 200 s are required to produce a cubic domain with 180^3 voxels, containing 1000 as well as 3000 polyhedra.

2.3. Extensions of the model and results

The proposed method can be easily extended. Periodic boundary conditions can be imposed, as in Fig. 1b,c: the vicinity graph of the grid is simply made periodic before the calculations. Edge effects are suppressed by this process, and infinite media can be simulated. This type of periodic simulation is very useful for further finite element computations with periodic boundary conditions.

Grain shape anisotropy can be generated from any deformation of the distance function (Fig. 2a). Thus are reproduced structures as obtained by a rolling process. Notice that it would be difficult to generate such anisotropic textures from standard computational geometry procedures, since a Poisson point process remains Poisson (and, therefore, isotropic) after any transformation of coordinates by affine transformations. Our construction based on distance function does not present this drawback. If a phase, or a component, is randomly assigned to each grain according to a given distribution, a multiphase polycrystal is generated. The assignation can be made uniform over space, or can be made according to an underlying random medium. In the last case, the phases are assigned non independently to the different polyhedra. This is obtained by assigning to every center a color (or label) according to a map generated by a second image. The color of any germ is then assigned to every voxel of the polyhedron that it generates. This differs from standard simulations, where the assignation of grains is made randomly, and independently for any pair of grains. An example is provided in Fig. 2b, where the map was produced by

the simulation of a color dead-leaves model (Jeulin, 1989), while in Fig. 3 the phases are assigned without any spatial correlation.

Finally, the distribution of grains can be made more regular, as compared to the standard Voronoï model: a minimal distance r between centers can be introduced, or

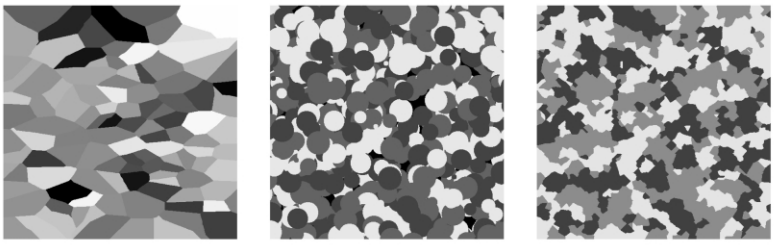

(a) Anisotropic grains obtained by deformation of the distance function.

(b) Assignation of a phase to each grain (right) from a realisation of a random multiphase dead-leaves model (left)

Fig. 2. Extension of the model.

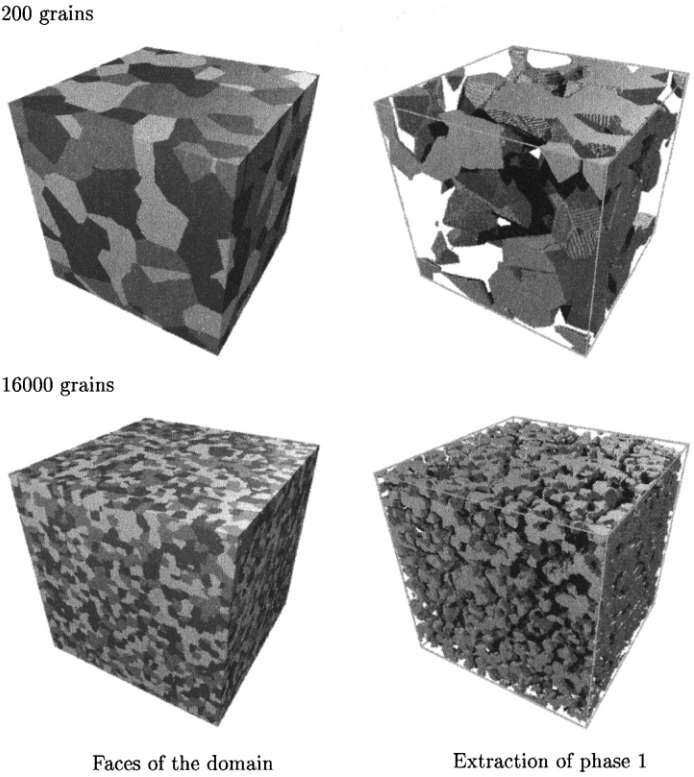

Fig. 3. Two-scale simulations of multiphase polycrystals. Grains are uniformly distributed over three phases, independently on each grain. Cubic domain (250^3 voxels) with periodic boundary conditions. A differently grey level is assigned to each phase.

more generally, a repulsion kernel (containing no other germ) can be given around every point of the process. In the last case, the location of centers is made sequentially, using an additional 3D image which records the forbidden locations. In this way, grains with a low size are eliminated and the distribution of the grain volumes is made much more uniform (Fig. 4b), as compared to the purely random case (Fig. 4a). This is interesting for investigating the effect of the dispersion of the grain volumes on the behavior of polycrystals.

3. Model for the single- and polycrystal

3.1. Single crystal

It is assumed that slip is the predominant deformation mechanism and that Schmid's law is valid. The resolved shear stress can then be used as a critical variable to evaluate the inelastic flow. A viscoplastic framework is chosen, in order to avoid the problems related with the determination of the active slip systems in plastic models. A threshold is introduced both in positive and negative directions on each slip system: 12 octahedral slip systems will be used for FCC materials. Two variables are defined for each slip system s, r^s and x^s, corresponding respectively to isotropic hardening (expansion of the elastic domain), and kinematic hardening (translation of the elastic domain). A system will be active provided its resolved shear stress τ^s is greater than $x^s + r^s$ or less than $x^s - r^s$ and the slip rate will be known as long as stress and the hardening variables are known. The state variables used to define the evolution of r^s and x^s are the accumulated slip v^s for isotropic hardening and the variable α^s for kinematic hardening. Knowing the stress tensor applied to the grain g, $\underline{\sigma}^g$ the resolved shear stress for system s can be classically written according to (2), $\overrightarrow{n}^s$ and $\overrightarrow{m}^s$ being respectively, for the system s, the normal to the slip plane and the slip direction in this plane. The hardening variables x^s and r^s can then be expressed

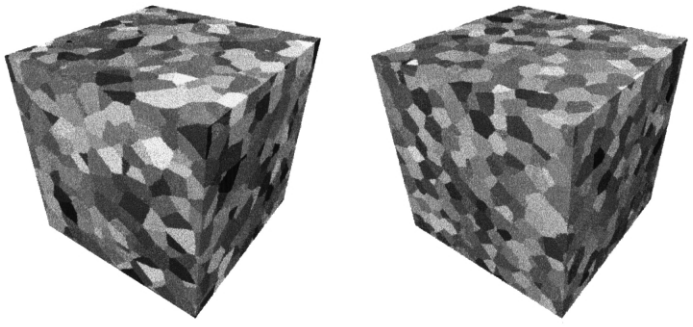

1000 grains on a Poisson point process

1400 grains located with a repulsion (sphere with radius $r = 20$)

Fig. 4. Voronï polyhedra: display of faces of a cubic domain (250^3 voxels) with periodic boundary conditions. A random grey level is assigned to each grain.

as a function of α^s and v^s following (3), their actual values allowing then to compute the viscoplastic slip rate $\dot{\gamma}^s$, the viscoplastic strain rate tensor $\dot{\underset{\sim}{\varepsilon}}^g$ (4), and the hardening rules [(5) and (6)]. The present formulation gives a saturation of the hardening in both monotonic and cyclic loading, and takes into account the interactions between the slip systems, through matrix h_{rs}, as in (Kocks and Brown, 1966). Nine material-dependent coefficients are involved in the model (E, v, K, n, c, d, R_0, Q, b).

$$\tau^s = \underset{\sim}{\sigma}^g : \underset{\sim}{\mathbf{m}}^s = \frac{1}{2}\underset{\sim}{\sigma}^g : \left(\vec{n}^s \otimes \vec{m}^s + \vec{m}^s \otimes \vec{n}^s\right) \tag{2}$$

$$x^s = c\alpha^s;\ r^s = R_0 + Q\sum_r h_{rs}\left\{1 - \mathrm{e}^{-bv^r}\right\} \tag{3}$$

$$\dot{\gamma}^s = \dot{v}^s \mathrm{sign}(\tau^s - x^s);\ \dot{\underset{\sim}{\varepsilon}}^g = \sum_s \underset{\sim}{\mathbf{m}}^s \dot{\gamma}^s \tag{4}$$

$$\dot{v}^s = \left\langle \frac{|\tau^s - x^s| - r^s}{K} \right\rangle^n \text{ with } \langle x \rangle = \mathrm{Max}(x, 0) \text{ and } v^s(t=0) = 0 \tag{5}$$

$$\dot{\alpha}^s = \dot{\gamma}^s - d\alpha^s \dot{v}^s \text{ with } \alpha^s(t=0) = 0 \tag{6}$$

Such a formulation (Cailletaud, 1987; Méric et al., 1991) is an extension of the classical crystallographic approach for single crystal modeling in plasticity or in viscoplasticity [see for instance (Taylor, 1938; Mandel, 1965; Asaro, 1983)]. Other more recent models belong to the same class, they were also developed in the eighties (Jordan and Walker, 1984; Swanson and Bill, 1985; Dame and Stouffer, 1986; Busso, 1990) to correctly represent the stress–strain behavior of superalloy single crystals. Due to the saturation of the hardening and the presence of kinematic hardening, the present model is valid for the simulation of cyclic loadings. It has been extensively used for single crystal modeling including Finite Element simulations.

3.2. Transition rules for the polycrystal

In a polycrystalline aggregate, one phase may be characterised by its shape, size, crystallographic orientation, location with respect to the surface of the material, etc. Most of the models usually specified for polycrystals made of equiaxial grains retain only the crystallographic orientation (Beaudoin et al., 1993; Staroselski and Anand, 1998; Mika and Dawson, 1999), and put in the same *crystallographic phase* all the grains having the same orientation. The alloy is then considered as a n-phase material, each phase being defined by a set of Euler angles, and the model will then be used to describe the mean behavior of all of them.

The oldest models proposed to obtain local stresses and strain in plasticity use simple assumptions like (i) uniform plastic strain (Taylor, 1938), (ii) uniform stress, (iii) uniform total strain (Lin, 1957). Nevertheless, it is generally admitted that, for

the case of polycrystals, the self-consistent scheme is a good candidate to schematically represent the phase interaction. The application in plasticity has been developed by Hill (1965), after the work done by Kröner on the elastic accomodation (Kröner, 1961) or Budianski and Wu (1962) who applied Eshelby solution for the problem of an ellipsoidal inclusion in an infinite medium (Eshelby, 1957). The case of viscoplastic behavior was treated by Hutchinson (1966). The problem can be written in terms of rates, allowing the computation of the local stresses $\underset{\sim}{\sigma}^g$ if the global stresses and strains and the local strain are known (7), by means of a fourth-order tensor $\underset{\approx}{\mathbf{L}}^*$ (8):

$$\dot{\underset{\sim}{\sigma}}^g = \dot{\underset{\sim}{\sigma}} + \underset{\approx}{\mathbf{L}}^* : \left(\dot{\underset{\sim}{\varepsilon}} - \dot{\underset{\sim}{\varepsilon}}^g\right) \tag{7}$$

with:

$$\underset{\approx}{\mathbf{L}} = \frac{1}{V}\sum_V \underset{\approx}{\mathbf{L}}^g : \left(\underset{\approx}{\mathbf{L}}^* + \underset{\approx}{\mathbf{L}}^g\right)^{-1} : \left(\underset{\approx}{\mathbf{L}}^* + \underset{\approx}{\mathbf{L}}\right) \tag{8}$$

where $\underset{\approx}{\mathbf{L}}$ characterises the incremental behavior of the equivalent medium, and $\underset{\approx}{\mathbf{L}}^g$the tangent behavior of each grain. If elasticity is uniform, the same model is valid with the local and macroscopic plastic strains. On the other hand, in the case of spherical phases, isochoric plasticity and proportional loading path, the model has a simplified expression (Berveiller and Zaoui, 1979). The relation (9) summarises the results given by several models, according to the definition of α, with a specific mention to $\alpha = 1$ (Kröner, 1961), or to (10) involving the overall equivalent stress Σ in uniaxial tension and the plastic part of the overall strain tensor E^p (Berveiller and Zaoui, 1979):

$$\underset{\sim}{\sigma}^g = \underset{\sim}{\sigma} + \alpha\mu\left(E^{\mathrm{p}} - \underset{\sim}{\varepsilon}^{\mathrm{pg}}\right) \tag{9}$$

with:

$$\frac{1}{\alpha} = 1 + \frac{3\mu E^{\mathrm{p}}}{2\Sigma} \text{ and } E^{\mathrm{p}} = \left\langle \underset{\sim}{\varepsilon}^{\mathrm{pg}} \right\rangle \tag{10}$$

From a physical point of view, the previous rule simply shows that a local plastic strain decreases the local stress, whereas the stress redistribution related to plastic accomodation tends to decrease for larger plastic strains. Many other works having used transition rules for polycrystal can be referenced (Beradai et al., 1987; Weng, 1987, 1993; Hess, 1993). The transition can also be expressed by a phenomenological model, and identified from finite element computation (Cailletaud and Pilvin, 1994; Pilvin, 1996):

$$\underset{\sim}{\sigma}^{g} = \underset{\sim}{\sigma} + \mu\left(\underset{\sim}{\beta} - \underset{\sim}{\beta}^{g}\right) \tag{11}$$

The new variable $\underset{\sim}{\beta}^{g}$ has a non linear evolution, depending on the local plastic strain in grain g, and $\underset{\sim}{\beta}$ is its mean for the aggregate. This approach no longer assumes that the stress is uniform in the equivalent homogeneous medium, and can be easily calibrated for cyclic loadings. Nevertheless, additional coefficients have to be introduced, which are not necessary in (9). Since the loading path in the present paper is just a tension, Berveiller–Zaoui model (BZ) will be chosen as the reference for the polycrystal behavior. The following coefficients are then used:

— isotropic elastic behavior: $E = 196000$ MPa, $v = 0.3$
— viscous effect in (5) and (6): $K = 10$ MPa.s$^{1/n}$, $n = 25$
— kinematic hardening in (3): $c = 1600$ MPa, $d = 40$
— isotropic hardening in (3) and (4): $R_0 = 111$ MPa, $Q = 35$ MPa, $b = 7$

4. Numerical implementation

4.1. Integration of the constitutive equations

The crystal plasticity models are implemented in the F.E. code ZéBuLoN, written in C++ (Besson and Foerch, 1998). Many constitutive equations are implemented in this code; from a numerical point of view, the crystal plasticity models can be considered as classical macroscopic models (Besson et al., 1998). For the single crystal, the state variables retained for the integration of the constitutive equations are the elastic strain tensor, the accumulated slip v^s and the kinematic variable α^s on each slip system. In the case of a FCC single crystal, 12 slip systems are considered, so that there are $(6+2\times12)$ variables for each Gauss point. For the polycrystal, a variable defining the intergranular hardening has also to be considered [either $\underset{\sim}{\varepsilon}^{g}$ used in (9) or $\underset{\sim}{\beta}^{g}$ introduced in (11), depending on the scale transition rule], so that, for P FCC grains, the number of variables is $(6+6\times P+2\times12\times P)$. The integration of the system is made by means of a theta–method, solved with a local Newton problem, for the models with a low number of variables (less than 100), but the code switches to Runge-Kutta methods for a large number of variables (using $P=200$ leads for instance to 6006 variables on each integration point). The consistent tangent matrix is obtained numerically in the Newton solution of the theta-method problem (Simo and Taylor, 1985; Cailletaud and Chaboche, 1996), and a BFGS algorithm is used at the global level together with the Runge-Kutta integration.

It has to be noted that the code has two original capabilities to applied loading paths on RVE's:

- A special RVE element, in which the degrees of freedom are the components of the strain tensor, and the reactions the stresses (the matrix [B] of the derivative of the shape functions is simply identity). This element can be included in a

F.E. computation, but the calculations are about 10 times faster than the corresponding computations with a regular finite element

- A simulator (ZSeT/ZéBuLoN-8, 1999) which consists in an independent piece of code acting on the material library, and with a fast numerical treatment of the loading (strain partition between elastic and plastic strain), so that the CPU time is again 10 times smaller than with the RVE element.

These capabilities are used to calibrate the material parameters, inside an optimisation loop, or simply to make the simulation, as in the present case: the reference tensile curves made with the self–consistent polycrystal model are produced with the RVE element.

4.2. Parallel computation

Many time-steps are needed, since the local loading paths are highly non-proportional. As the global problem is quite large for a single workstation, the parallel version of the code is used (Feyel et al., 1997; Feyel, 1998). The solution of the system is obtained by subdomains, with the FETI method (Fahrat and Roux, 1994) and the interprocessor communications are managed by use of the PVM or MPI libraries. The jobs are performed on an IBM-SP2 11-node parallel computer.

4.3. Representation of the RVE

The polycrystalline volume is discretised as a regular cubic mesh, and the material properties are distributed on each Gauss point. The actual aggregate in the calculation differs then slightly from the initial one. The main problem of such an approach is that the grain boundary is not a collection of oblique flat faces, but presents many steps. This problem will be discussed later on. Let us just note that in the present calculation we have tried to put as many integration points as possible in each grain, in order to have a reasonable general description of the stress and strain gradients in the grains. A balance must be found between two opposite requirements (i) having a large number of grains to have a representative microstructure, (ii) having enough Gauss points in each grain. A good compromise was found with 238 grains in a $18\times18\times18$ mesh made of 20-node-elements with $3\times3\times3$ integration (157464 Gauss points). The mean value is then 661 Gauss points in each grain. In other works dealing with polycrystals, i.e. for computation of aggregates containing a sufficient number of grains, the most discretised structures propose 576 points per grain in (Mika and Dawson, 1999) for a total number of 300 crystals. This large number of points is illustrated in Fig. 5, where the volume of each grain is plotted as the distance to the surface of the aggregate (each finite element is assigned a volume equal to 1, the volume of the whole structure is then $18^3 = 5832$). As many grains are cut by the "numerical machining" when the cube including 238 grains is extracted from the original aggregate, most of the small grains are near the surface. It can also be seen that more than 50 grains have more than 1000 Gauss points, and more than 100 grains have more than 500 Gauss points.

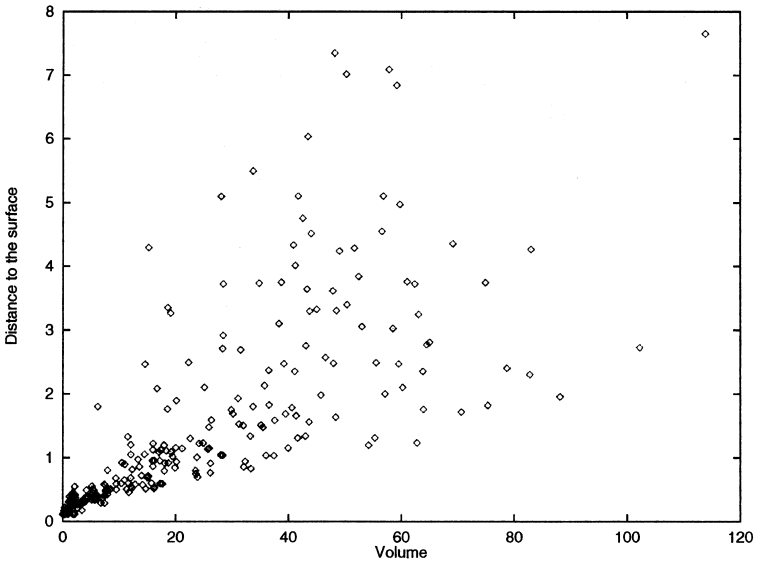

Fig. 5. Volume of the grain *vs* distance to the surface of the aggregate.

5. Validation of the numerical model

5.1. Construction of the aggregate

Two strategies are tested to generate the set of grain orientations. The first one considers 40 orientations, designed to provide a cubic symmetry (Cailletaud and Pilvin, 1994; Pilvin, 1996). Those orientations can be classified into four different "base orientations" only, which are defined in the standard triangle, each of them allowing the generation of ten grains by rotation around the last free Euler angle. All the grains generated from a given base orientation are then equivalent under tensile loading in a self consistent approach. Other orientation sets have simply been generated by a random generation of Euler angles.

Several polycrystalline aggregates have been computed that allow us to compare the responses of the F.E. model and of the self–consistent approach for different geometrical and texture realisations. In the following notation, each code m1 to m5 corresponds to a new geometrical aggregate. The first number specifies the number of real grains, the second one refers to the number of phases:

i. microstructure (m1-238-40) with 238 grains whose crystallographic orientations are taken from the 40-phase set,
ii. microstructure (m1-238-238) with 238 grains with 238 random crystallographic orientations,
iii. microstructure (m3-200-40) with 200 grains and the same 40-phase set,
iv. microstructure (m4-200-200) with 200 grains and 200 random crystallographic orientations (geometrical realisation 1),

v. microstructure (m5-200-200) with 200 grains and 200 random crystallographic orientations (geometrical realisation 2).

All the computations have been made with a $18\times18\times18$ mesh. Each aggregate is described by a mesh made of $18\times18\times18$ quadratic cubic elements (20 nodes and 27 Gauss points per brick). The spatial distribution of the phases is shown in Fig. 6; (m4) is studied in detail in the second part of the article (Barbe et al., 2001). Aggregates with 10 or 40 grains have also been considered, but they do not produce an isotropic aggregate, since the volume fraction of each grain is not the same. Therefore, the results are not reported here.

For the case of m1-238-40, the volume fraction of each base orientation has been controlled, it is respectively 25.09, 25.04, 24.97 and 24.90%. Nevertheless, the individual contribution of each ten "children" of each base orientation cannot be accurately set to 25%, since it depends on the geometry of a low number of grains. The volume fraction for each phase varies between 0.0073 and 0.0546%. For m3-200-40, there is no special control on any volume fraction, leading to a minimum value of 22.67%, and a maximum value of 27.15% for the base orientations.

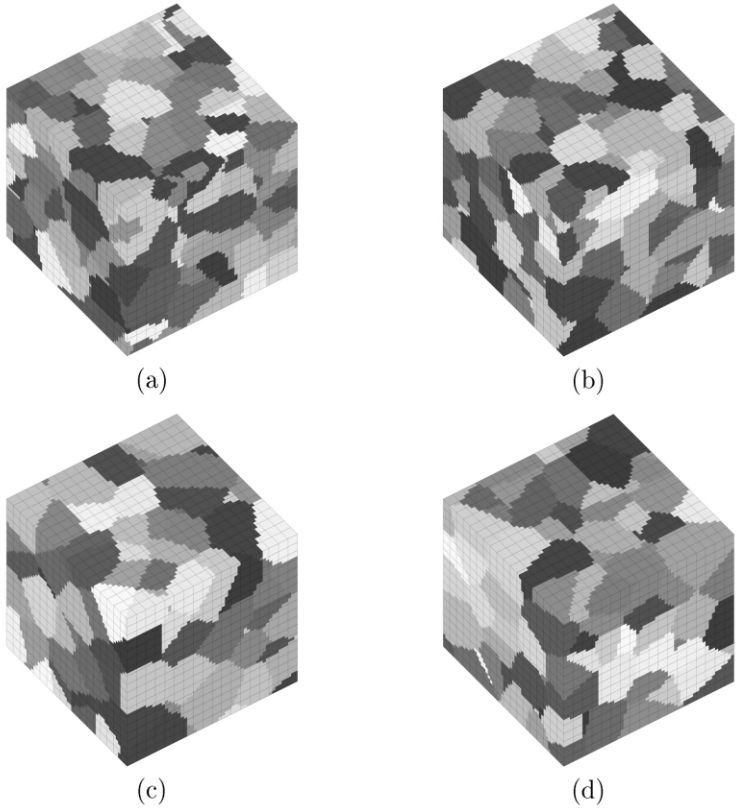

Fig. 6. F.E. representations of all the aggregates simulated under isovolumic conditions of load: (a) m1, (b) m3, (c) m4, (d) m5.

5.2. Influence of the geometry and of the texture

All these microstructures have been loaded in tension, in order to reach an axial strain of 1.5%, with isovolumic conditions (lateral strain −0.75%). Reference computations have also been performed with BZ model, by taking the same crystallographic orientations and the same volume fraction for each phase. Typical results are shown in Fig. 7a,b,c where the average values of each stress and strain component on the whole mesh have been used to draw the macroscopic curve coming from the F.E. For the sake of clarity, since the discrepancy between the various BZ responses remains low, the only curves plotted for the BZ model are the solutions obtained with m1-238-40 microstructure (BZ-238-40), that is, with the volume fractions read in m1-238-40, and the reference solution with the same amount of the 40 special orientations (BZ-40-40).

In the tensile direction (Fig. 7c), the discrepancy between the various computations is very low (less than 5%), the BZ model appearing as a higher bound. The two BZ computations are the same, due to the good balance between the various base orientations. It has to be noted that the sensitivity to the different assumptions made in the computations is larger for the lateral stresses (Fig. 7a and b). The difference between the two BZ simulations in these planes is significant, the result on the real microstructure m1-238-40 being anisotropic (116 MPa in x direction, 132 MPa in y direction). The larger discrepancy is found for m1-238-40 microstructure, on xx component of the stress (around 8%), while the best isotropy is obtained for the m5-200-200 microstructure.

The present results demonstrate that 200 is a reasonable number of grains, the mean behavior being almost the same for any kind of distribution. The choice of a random set of orientation seems to provide a good quality aggregate. In the following, the 40-phase distribution will be used for the comparison of the F.E. with the BZ model, since it offers the opportunity to compare the responses of individual grains which have exactly the same orientation in different positions (and with different neighbors) in the aggregate. Besides, we will switch to randomly oriented grains for further analysis of the intragranular behavior.

5.3. Influence of the element interpolation

Several microstructures have been computed using two different interpolation levels in the element: each aggregate is represented either with quadratic elements made of 20–node–bricks containing 27 integration points, or with linear elements made of 8–node–bricks containing 8 integration points. The structures have been generated in such a way that the number of integration points in a given microstructure remains the same whether the elements are quadratic or linear. In this type of computations, the linear meshes usually appear to be too stiff. This is illustrated in Fig. 8, which shows the macroscopic stress–strain curve for the case of m1-238-40 microstructure. The difference is still more important on a transgranular level, the quadratic interpolation allowing a finer description of the local fields. As demonstrated by Fig. 9a,b, which shows the contour plot of the amount of plastic slip, after a 1.5% tension, there is a qualitative agreement between the two calculations

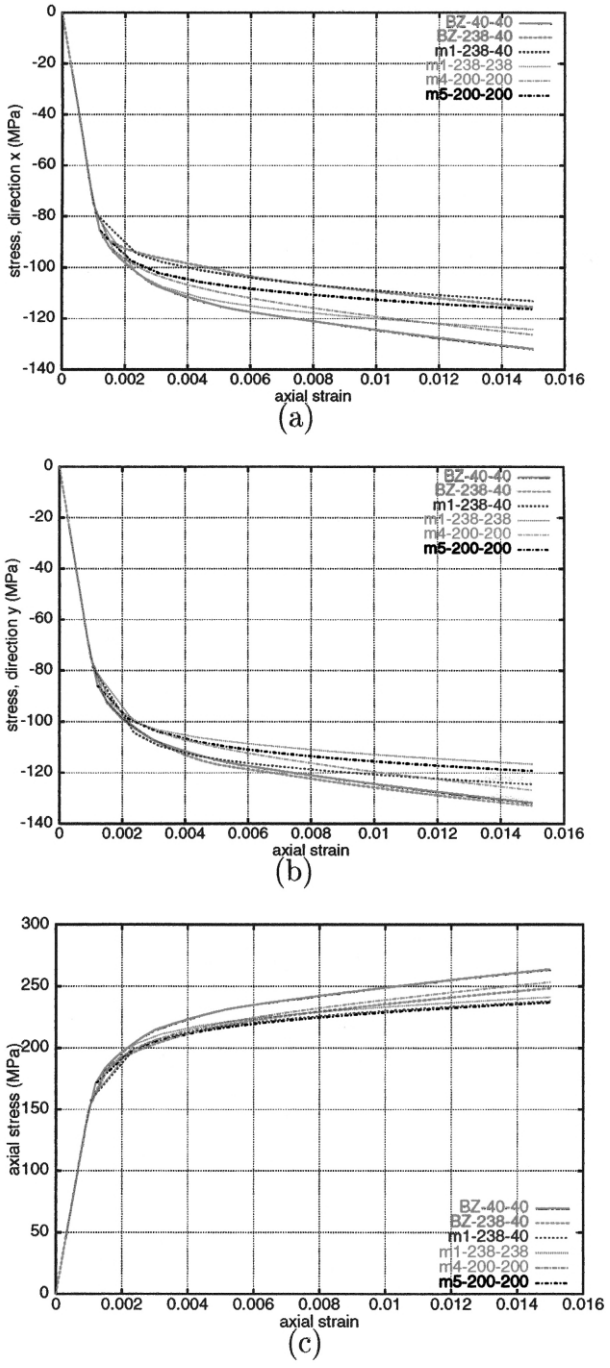

Fig. 7. Comparison of the mean stress-strain response of four aggregates subjected to isovolumic loading conditions: (a) stress in direction x, (b) stress in direction y, (c) axial stress.

concerning the zone of strain concentration, nevertheless the values are quite different: the range is (0.00545–0.0858) for the linear mesh, while (0.00005–0.1219) is obtained with the quadratic interpolation.

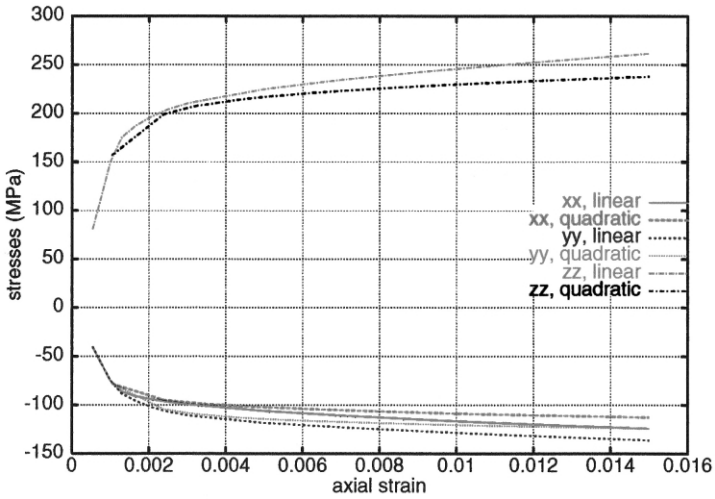

Fig. 8. Effect of the interpolation mode on the mean stress-strain response of three aggregates subjected to isovolumic loading conditions, for *m1-238-40*

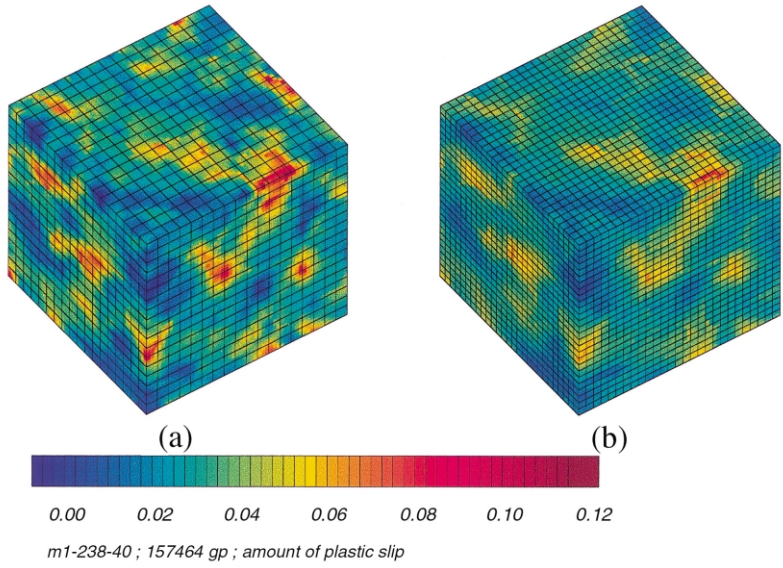

Fig. 9. Effect of interpolation mode on the local slip activity of the m1-238-40 distribution subjected to isovolumic loading conditions: (a) 5832 quadratic elements, 157464 integration points, (b) 19683 linear elements, 157464 integration points.

5.4. Influence of the size of the mesh

In order to check the convergence of the mean stress–strain response relatively to the number of elements used to represent a given aggregate, the simulation of a simple tensile test on microstructure (m4-200-200) has been performed with four meshes of different sizes:

- $16\times16\times16$ quadratic elements, i.e. 110592 integration points,
- $18\times18\times18$ quadratic elements, i.e. 157464 integration points,
- $20\times20\times20$ quadratic elements, i.e. 216000 integration points,
- $24\times24\times24$ quadratic elements, i.e. 373248 integration points.

Only the onset of plasticity was computed in the bigger meshes (20^3 and 24^3 elements), so that the comparison is made for a low total strain (0.2%). It is not surprising to check that the global response is the same for all the meshes, as

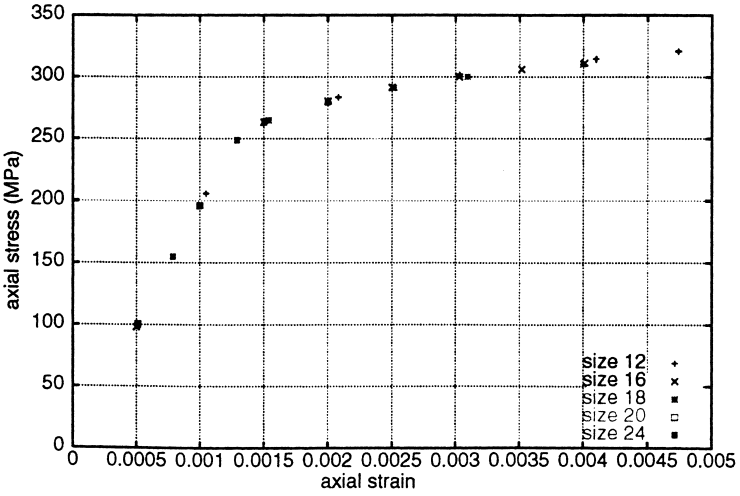

(a)

elt number	min	max
12^3	194.80	411.02
16^3	191.42	464.42
18^3	185.68	456.90
20^3	184.19	470.94
24^3	180.37	470.91

(b)

Fig. 10. Effect of the mesh size on the response of the m4-200-200 microstructure after a 0.2% tension: (a) axial stress vs axial strain, (b) min and max local values of the axial stress.

shown in Fig. 10, since it is known that a relatively low number of elements (typically 12^3) provides the proper answer. On the other hand, the local response still depends on the size of the mesh in the investigated range, as summarised in Fig. 10b, which contains the min and max values of the axial stress in the aggregate. This effect can be precised by the observation of the contour plots of the axial stress in

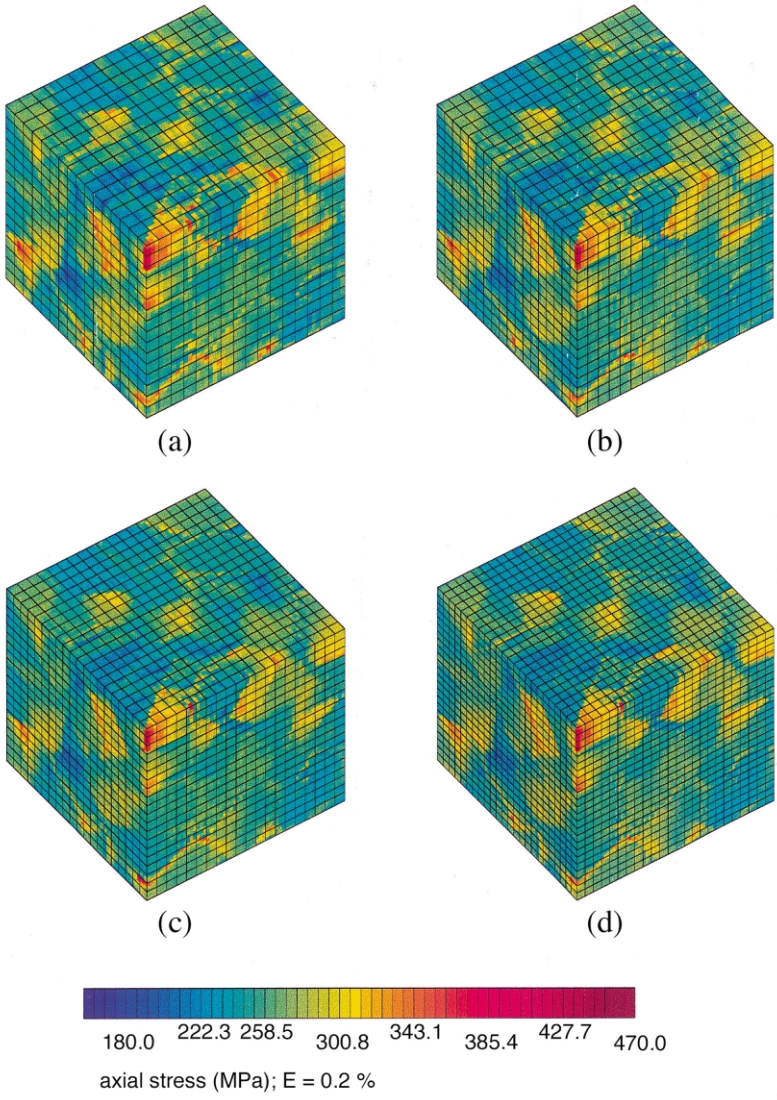

Fig. 11. Effect of the mesh size on the local behaviour of the m4-200-200 microstructure after 0.2% simple tension: (a) 16^3 quadratic elements, (b) 18^3 quadratic elements, (c) 20^3quadratic elements, (d) 24^3quadratic elements

Fig. 11 and of the cumulated slip on all the slip systems, in Fig. 12. These last contours are specially significant, since they show the organisation of the deformation patterns independently of the local microstructure (i.e. localisation zones crossing the grain boundaries). These patterns become finer when the precision of the mesh increases.

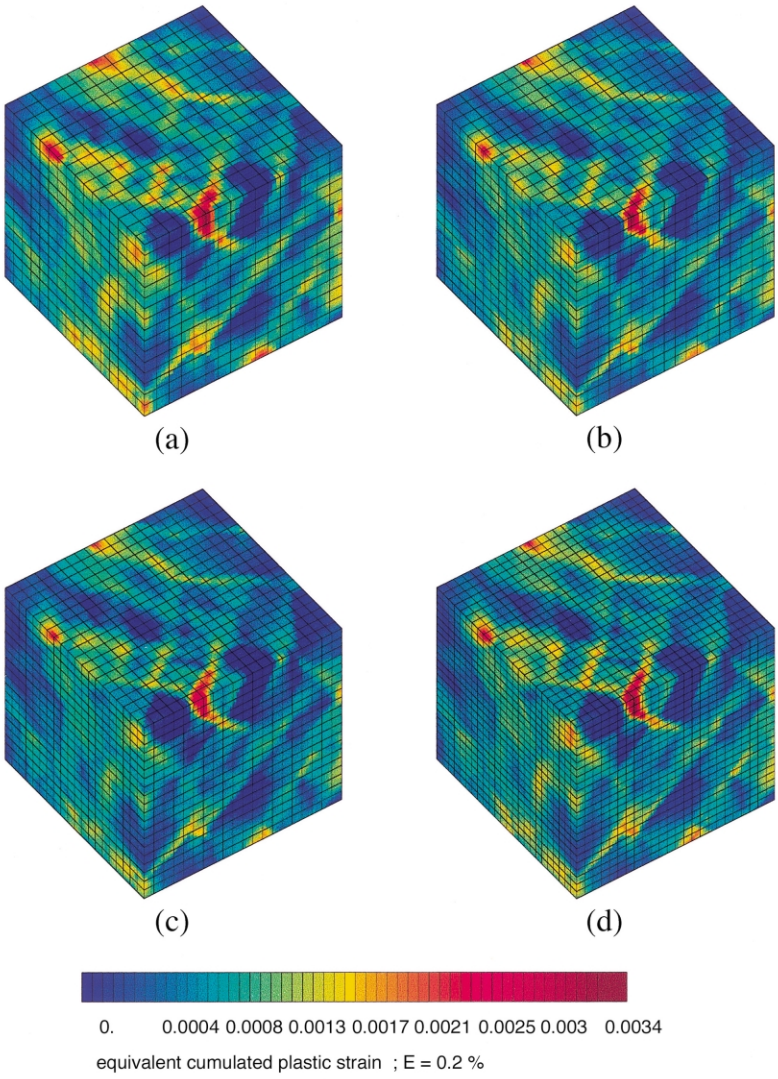

Fig. 12. Effect of the mesh size on the local behaviour of the *m4-200-200* microstructure after 0.2% simpler tension: (a) 16^3 quadratic elements, (b) 18^3 quadratic elements, (c) 20^3quadratic elements, (d) 24^3quadratic elements

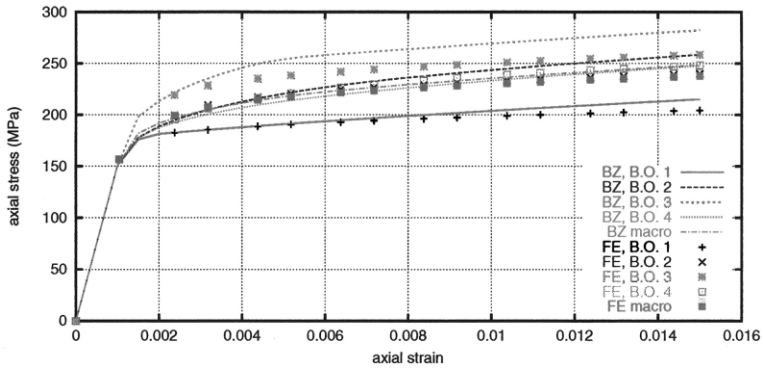

Fig. 13. Stress-strain curves for each basic orientation of the standard triangle for the m1-238-40 microstructure tensile strained at 1.5% with isovolumic conditions.

5.5. *Local comparison with the self–consistent model*

The previous comparisons between F.E. and BZ model only concern the global response. The curve in Fig. 13 shows the comparison of the tension curves obtained for each "base orientation" of the m1-238-40 microstructure. The curve is obtained from the F.E. result by averaging the value of the axial stress and strain components in four classes of grains coming from the same initial orientation, as explained in Section 5.1. The agreement is correct, but not as good as for the global loading. This difference is a first step toward the high level of heterogenity which will be discussed in the second part of the article.

6. Conclusion

The present paper describes a numerical environment for studying the mechanics of crystalline solids on a microscale. The main results concern the validation of the different tools and of the numerical techniques. Synthetic microstructures can be created to represent material elements with a controlled number of grains. Prescribed textures can therefore be applied to the aggregate. The first purpose of this paper was to propose a solution to get a representative microstructure for an isotropic RVE. It is not surprising to see that it is better to work with as many grains as possible. On the other hand, it is shown that the results obtained are quite comparable with a random microstructure or a polycrystal with a reduced number of orientations, chosen to reproduce an isotropic behavior. In the following part (Barbe et al., 2001), we will work with at least 200 grains, and a random microstructure. The influence of the mesh size has also been considered. It can be observed that, since small strain assumption is used in the paper, quadratic elements give better results than linear ones. Full integration in the quadratic elements ($3\times3\times3$ integration points per element) gives the opportunity to have a better description of

the local geometry and remains acceptable compared to reduced elements. With our conditions of loads, the overall strain is not too high so that the elastic strain cannot be neglected and the definition of hydrostatic stresses is still correct. Using a $18\times18\times18$ mesh corresponds to a good quality-price ratio, as confirmed by computations performed with $20\times20\times20$ and $24\times24\times24$ elements. In the last section of the paper, the F.E. model is also validated with respect to the self–consistent approach. The agreement between the macroscopic responses is good, with only 2% discrepancy in terms of stress for a given strain. The heterogenity on the phases is also correctly represented, even if the difference for the two types of modeling reaches now 8% for the local axial stresses. In the following part, the numerical procedure will be used to compute an aggregate made of $18\times18\times18$ elements in order to provide a numerical evaluation of the various stress and strain fields on a microscale, specially concerning the intragranular heterogenity, which is essential to understand damage initiation.

References

Asaro, R.J., 1983. Crystal Plasticity. J. Appl. Mech. 50, 921–934.

Bachu, V., Kalidindi, S.R., 1998. On the accuracy of the predictions of texture evolution by the finite element technique for fcc polycrystals. Mat. Sci. Engng. A257, 108–117.

Barbe, F., Forest, S., Cailletaud, G., 2001. Intergranular and intragranular behavior of polycrystalline aggregates. Part 2: Results. Int. J. Plasticity 17, 537–563.

Beaudoin, A.J., Dawson, P.R., Mathur, K.K., Kocks, U.F., 1995. A hybrid finite element formulation for polycrystal plasticity with consideration of macrostructural and microstructural linking. Int. J. Plasticity 11, 501–521.

Beaudoin, A.J., Mathur, K.K., Dawson, P.R., Johnson, G.C., 1993. Three-dimensional deformation process simulation with explicit use of polycrystal plasticity models. Int. J. Plasticity 9, 833–860.

Becker, R., 1991. Analysis of texture evolution in channel die compression — I. Effects of grain interaction. Acta Metall. Mater. 39 (6), 1211–1230.

Becker, R., Panchanadeeswaran, S., 1995. Effects of grain interactions on deformation and local texture in polycrystals. Acta Metall. Mater. 43 (7), 2701–2719.

Beradai, C., Berveiller, M., Lipinski, P., 1987. Plasticity of metallic polycrystals under complex loading path. Int. J. Plasticity 3, 143–162.

Bertram, A., Boehlke, T., Duderstadt, F., Kraska, M., 1998. Berechnung der Texturentwicklung und verformungsinduzierten Anisotropie metallischer Polykristalle. In: GAMM Annual meeting, Bremen. to appear in ZAMM.

Berveiller, M., Zaoui, A., 1979. An extension of the self–consistent scheme to plastically flowing polycrystal. J. Mech. Phys. Solids 26, 325–344.

Besson, J., Foerch, R., 1998. Object-oriented programming applied to the finite element method. Part I. General concepts. Revue Européenne des Éléments Finis 7 (5), 535–566.

Besson, J., Leriche, R., Foerch, R., Cailletaud, G., 1998. Object-oriented programming applied to the finite element method. Part II. Application to material behaviors. Revue Européenne des Éléments Finis 7 (5), 567–588.

Budianski, B., Wu, T.T., 1962. Theoretical prediction of plastic strains of polycrystals. In: Proceedings of the 4th US National Congress on Applied Mechanics. pp. 1175–1185.

Busso, E.P., 1990. Cyclic Deformation of Monocrystalline Nickel Aluminide and High Temperature Coatings. PhD thesis, MIT.

Cailletaud, G., 1987. Une Approche micromécanique Phénoménologique du Comportement Inélastique des Métaux. PhD thesis, Université Pierre et Marie Curie, Paris 6.

Cailletaud, G., Chaboche, J.L., 1996. Integration methods for complex plastic constitutive equations. Comput. Meth. Appl. Mech. Engng. 133, 125–155.
Cailletaud, G., Pilvin, P., 1994. Utilisation de modèles polycristallins pour le calcul par éléments finis. Revue Européenne des Éléments Finis 3 (4), 515–541.
Canova, G.R., Wenk, H.R., Molinari, A., 1992. Deformation modelling of multi-phase polycrystals: case of quartz-mica aggregate. Acta Metall. Mater. 40 (7), 1519–1530.
Dame, L.T., Stouffer, D.C., 1986. Anisotropic Constitutive Models for Nickel Base Single Crystal Alloys: Development and Finite Element Implementation. Cr-175015, NASA.
Dawson, P.R., Marin, E.B., 1998. Computational mechanics for metal deformation processes using polycrystal plasticity. Adv. Appl. Mech. 34, 77–169.
Decker, L., Jeulin, D., 2000. Simulation 3D de matériaux aléatoires polycristallins. Revue de Métallurgie-CIT/Science et Génie des Matériaux, Feb., 271–275.
Engel, J.J., 1978. Modélisation du Comportement Global des Métaux en Plasticité et en Viscoplasticité. PhD thesis, Ecole Nationale Supérieure des Mines de Paris.
Eshelby, J.D., 1957. The determination of the elastic field of an ellipsoidal inclusion, and related problems. Proc. R. Soc. London A 241, 376–396.
Fahrat, C., Roux, F.X., 1994. Implicit parallel processing in structural mechanics. Comput. Mech. Adv. 2 (1).
Feyel, F., 1998. Application du Calcul Parallèle aux Modèles à Grand Nombre de Variables Internes. PhD thesis, Ecole Nationale Supérieure des Mines de Paris.
Feyel, F., Cailletaud, G., Kruch, S., Roux, F.X., 1997. Application du calcul parallèle aux modèles à grand nombre de variables internes. In: Colloque National en calcul de structures, Giens, France.
Gilbert, E.N., 1962. Random subdivisions of space into crystals. Ann. Math. Stat. 33.
Gotoh, M., 1978. A finite element formulation for large elastic–plastic deformation analysis of polycrystals and some numerical considerations on polycrystalline plasticity. Int. J. Num. Meth. Engng. 12, 101–114.
Gratin, C., 1992. Xlim3d: un Logiciel de Traitement d'Images Tridimensionnelles. Tech. Rep. N-9/92, Ecole des Mines de Paris.
Gratin, C., 1993. De la Représentation des Images au Traitement Morphologique d'Images Tridimensionnelles. PhD thesis, Ecole Nationale Supérieure des Mines de Paris.
Gratin, C., Meyer, F., 1992. Mathematical morphology in three dimensions. Acta Stereologica (Suppl.1), 551–558.
Harder, J., 1999. A crystallographic model for the study of local deformation processes in polycrystals. Int. J. Plasticity 15 (6), 605–624.
Harren, S.V., Asaro, R.J., 1989. Nonuniform deformations in polycrystals and aspects of the validity of the Taylor model. J. Mech. Phys. Solids 37, 191–232.
Havlićek, F., Kratochvil, J., Tokuda, M., Lev, V., 1990. Finite element model of plastically deformed multicrystal. Int. J. Plasticity 6, 281–291.
Havlićek, F., Tokuda, M., Hino, S., Kratochvil, J., 1992. Finite element method analysis of micro-macro transition in polycrystalline plasticity. Int. J. Plasticity 8, 477–499.
Hess, F., 1993. Anisotropic strain hardening in polycrystalline copper and aluminium. Int. J. Plasticity 9, 405–420.
Hill, R., 1965. Continuum micro-mechanisms of elastoplastic polycrystals. J. Mech. Phys. Solids 13, 89–101.
Hutchinson, J.W., 1966. Elastic–plastic behaviour of polycrystalline metals and composites. Proc. R. Soc. London A 319, 247–272.
Jeulin, D., 1989. Morphological modeling of images by sequential random functions. Signal Processing 16.
Johnson, W.A., Mehl, R.F., 1939. Reaction kinetics in processes of nucleation and growth. Trans. Am. Inst. Min. Engrs. 135, 416–458.
Jordan, E., Walker, K.P., 1984. Biaxial constitutive modeling and testing of single crystals at elevated temperature. In: Conference on Multiaxial Fatigue, Sheffield, UK.
Kalidindi, S.R., Bronkhorst, C.A., Anand, L., 1992. Crystallographic evolution in bulk deformation processing of FCC metals. J. Mech. Phys. Solids 40, 537–569.
Kocks, U.F., Brown, T.J., 1966. Latent hardening in aluminium. Acta Metall. 14, 87–98.
Kröner, E., 1961. Zur plastischen Verformung des Vielkristalls. Acta Metall. 9, 155–161.

Lin, T.H., 1957. Analysis of elastic and plastic strains of face centered cubic crystal. J. Mech. Phys. Solids 5, 143–149.
Mandel, J., 1965. Une généralisation de la théorie de la plasticité de W.T. Koiter. Int. J. Solids Structures 1, 273–295.
Méric, L., Cailletaud, G., Gaspérini, M., 1994. F.E. calculations of copper bicrystal specimens submitted to tension–compression tests. Acta Metall. 42 (3), 921–935.
Méric, L., Poubanne, P., Cailletaud, G., 1991. Single crystal modeling for structural calculations. Part 1: model presentation. J. Engng. Mat. Technol. 113, 162–170.
Meyer, F., 1990. Algorithmes à base de files d'attente hiérarchiques. Technical Report N46/90/MM, Ecole Nationale Supérieure des Mines de Paris.
Meyer, F., 1992. Un algorithme optimal de ligne de partage des eaux. In: Proceedings of the Fourth International Conference on Image Processing and its Applications, Maastricht, pp. 303–306.
Meyer, F., Beucher, S., 1990. Morphological segmentation. J. Visual Communication and Image Representation 1 (1), 21–46.
Mika, D.P., Dawson, P.R., 1999. Polycrystal plasticity modeling of intracrystalline boundary textures. Acta Mater. 47 (4), 1355–1369.
Mika, D.P., Dawson, P.R., 1998. Effects of grain interaction on deformation in polycrystals. Mat. Sci. Engng. A257, 62–76.
Pilvin, P., 1996. The contribution of micromechanical approaches to the modelling of inelastic behaviour. In: Pineau, A., Cailletaud, G., Lindley, T. (Eds.), Fourth international conference on biaxial/multiaxial fatigue, Vol. 1. ESIS, Saint-Germain, France, pp. 3–19.
Quilici, S., Cailletaud, G., 1999. F.E. simulation of macro-, meso- and micro-scales in polycrystalline plasticity. Comput. Mat. Sci. 16 (1–4), 383–390.
Ragnemalm, I., 1992. Fast erosion and dilation by contour processing and thresholding of distance maps. Pattern Recognition Letters 13 (3), 161–166.
Simo, J.C., Taylor, R.L., 1985. Consistent tangent operators for rate independent elasto-plasticity. Comput. Meth. Appl. Mech. Engng. 48, 101–118.
Staroselski, A., Anand, L., 1998. Inelastic deformation of polycrystalline face centered cubic materials by slip and twinning. J. Mech. Phys. Solids 46 (4), 671–696.
Swanson, G.A., Bill, R.C., 1985. Life prediction and constitutive models of engine hot section anisotropic materials. In: AIAA/SAE/ASME/ASEE 21th Joint Propulsion Conference, Monterey.
Takahashi, H., Fujiwara, K., Nakagawa, T., 1998. Multiple-slip work–hardening model in crystals with application to torsion-tension behaviors of aluminium tubes. Int. J. Plasticity 14 (6), 489–509.
Takahashi, H., Motohashi, H., Tokuda, M., Abe, T., 1994. Elastic-plastic finite element polycrystal model. Int. J. Plasticity 10 (1), 63–80.
Taylor, G., 1938. Plastic strain in metals. J. Inst. Metals 62, 307–324.
Teodosiu, C., Raphanel, J.L., Tabourot, L., 1991. Finite element simulation of the large elastoplastic deformation of multicrystals. In: Teodosiu, C., Raphanel, J.L., and Sidoroff, F. (Eds.), Proceedings of the International Seminar Mecamat'91: Large Plastic Deformations, Fundamental Aspects and Applications to Metal Forming, Fontainebleau, France, pp. 153–168.
Weng, G.J., 1987. Anisotropic hardening in single crystals and the plasticity of polycrystals. Int. J. Plasticity 3, 315–339.
Weng, G.J., 1993. A self-consistent relation for the time-dependent creep of polycrystals. Int. J. Plasticity 9, 181–198.
Yao, Z., Wagoner, R.H., 1993. Active slip in aluminium multicrystals. Acta Metall. Mater. 41, 451–468.
ZSeT/ZéBuLoN-8, 1999. User manual. EMP/LMR/NWNM/ONERA.